remote sensing

MDPI

Article

Are the Significant Ionospheric Anomalies Associated with the 2007 Great Deep-Focus Undersea Jakarta-Java Earthquake?

Dan Tao [1,2,*], Guangxue Wang [1,2], Jiayi Zong [1,2], Yuanzheng Wen [1,2], Jinbin Cao [3], Roberto Battiston [4,5] and Zhima Zeren [6]

[1] Key Laboratory of Earth Exploration and Information Techniques of Ministry of Education, Chengdu University of Technology, Chengdu, China; dan.tao@cdut.edu.cn; wangguangxue@stu.cdut.edu.cn; zongjiayi@stu.cdut.edu.cn; wenyuanzheng@stu.cdut.edu.cn

[2] College of Geophysics, Chengdu University of Technology, Chengdu, China; dan.tao@cdut.edu.cn; wangguangxue@stu.cdut.edu.cn; zongjiayi@stu.cdut.edu.cn; wenyuanzheng@stu.cdut.edu.cn

[3] School of Space and Environment, Beihang University, Beijing, China; jbcao@buaa.edu.cn

[4] Dipartimento di Fisica, Università di Trento, Trento, Italy; roberto.battiston@unitn.it

[5] Trento Institute for Fundamental Physics and Applications (TIFPA), National Institute for Nuclear Physics (INFN), Trento, Italy; roberto.battiston@unitn.it

[6] National Institute of Natural Hazards, Ministry of Emergency Management of China, Beijing, China; zrzm@seis.ac.cn

* Correspondence: dan.tao@cdut.edu.cn;

Abstract: This work is an attempt to critically analyze the correlation between great deep-focus undersea earthquake and possible ionospheric anomalies. The significant TEC (total electron content) spatial and temporal anomalies were detected over the epicenter of 2007 M_w7.5 Jakarta-Java earthquake, and they coincide well with the striking plasma anomalies in the ionosphere in-situ observed by the LEO satellite. The localization and synchronization of the disturbances during the earthquake suggest that these ionospheric anomalies are highly related to this undersea earthquake. In order to identify this correlation, we made efforts to distinguish seismo-associated signals from large electromagnetic noise due to natural non-seismic sources, artificial signals and geomagnetic activities. Nevertheless, the difficulties of this work should be recognized and approached with caution. For large undersea earthquakes, considering their focal depth and energy loss transmitted to the seafloor, seismically induced IAWs or AWs/AGWs due to pre-seismic ground vibrations or AWGs result from radon emission during the earthquake preparation phase could be responsible of the coupling between undersea earthquakes and ionospheric disturbances. The special (undersea and deep-focus) case study here provides us with valuable information on the study of lithosphere-atmosphere-ionosphere coupling process.

Keywords: undersea earthquake; seismo-ionospheric anomaly; lithosphere-atmosphere-ionosphere (LAI) coupling; infrasonic acoustic waves (IAWs); acoustic (AWs) and acoustic gravity waves (AGWs)

Citation: Lastname, F.; Lastname, F Lastname, F. Title. *Remote Sens.* **2022**, *14*, x. https://doi.org/10.3390/xxxxx

Academic Editor: Firstname Lastname

Received: date
Accepted: date
Published: date

Publisher's Note: MDPI stays neutral with regard to jurisdictional claims in published maps and institutional affiliations.

1. Introduction

Over the past decades, seismic anomalies occurring during (pre-, co- and post-) large earthquakes have been widely investigated. A large number of studies have been carried out both on ground and in space with different methodologies and physical quantities [1-33], they are essential to our understanding of the lithosphere-atmosphere-ionosphere (LAI) coupling process. Unlike the well-established co-seismic effects in the lithosphere

and upper atmosphere [34-42], the possible pre- and post-seismic phenomena in the ionosphere have not been fully confirmed.

Even though many seismic anomalies have been found in the ionosphere, this physical process of LAI coupling is still unclear and even controversial, and there are still plenty of issues or details that need to be carefully worked through. On the one hand, such studies rarely distinguish between inland and submarine seismic events, and mainly focus on the former. Although they have some similar characteristics in some ways, both on land and at sea, such as the increased gases and aerosol release in seismic regions and which in turn rises and affects the electromagnetic environment of the atmosphere [43-48], and seismically induced acoustic and gravity waves [28,29,49-57]. On the other hand, it is difficult to identify the earthquake associated effects due to the fuzzy background noises resulting from natural (such as volcanic eruptions, thunderstorms, tsunamis, etc.) and artificial non-seismic sources (such as communications facilities, power lines, explosions, etc.), besides solar and global geomagnetic perturbations. The main focus of this work is to study the possibility of ionospheric perturbations associated to a special (undersea and deep-focus) earthquake, i.e., the 2007 M_w7.5 Jakarta-Java Earthquake. Then we attempt to carefully eliminate background noises, and critically discuss possible physical mechanisms of this lithosphere-atmosphere-ionosphere coupling process.

In this study, in order to search for possible ionospheric disturbances during the large earthquake, we examine the global ionosphere maps (GIM) of the GPS TEC and the plasma data from the French DEMETER satellite. The GPS satellites transmit at two ultra-high frequencies (1575.42 and 1227.60 MHz) and provide an effective approach for monitoring the ionosphere. The data of GIM TEC, with $2.5^{\circ}\times5^{\circ}$ (Lat. × Long.) spatial resolution and 2h time interval, are obtained from the Jet Propulsion Lab (JPL) (https://cdaweb.gsfc.nasa.gov/sp_phys/). And DEMETER (Detection of Electro-Magnetic Emissions Transmitted from Earthquake Regions) satellite, with a quasi Sun-synchronous circular orbit at an altitude of ~710 km [58], can measure sensitively over seismically quiet and active regions. The plasma data that will be involved in the study are from payload ISL (Langmuir probe instrument) [59], IAP (Plasma analyser instrument) [60], ICE (Electric field instrument) [61] and IMSC (Search-coil magnetometer instrument) [58], respectively (https://sipad-cdpp.cnes.fr/).

2. The 2007 M_w7.5 Jakarta-Java Earthquake

The deep hypocentral (280 km) main shock (oblique-reverse type) with magnitude M_w7.5 occurred in the offshore Java island (5.86°S, 107.42°E) at 17:05:04 UTC on 8 August 2007. Figure 1 displays this earthquake location and its preparation zone, which estimated by Dobrovolsky formula $\rho = 10^{0.43 \cdot M}$ and here M is the magnitude [62]. From 24 July to 13 August, there are another three $M_w \geq 5.0$ earthquakes around the main shock. In detail, the M_w5.3 earthquake occurred on 15 days before the main shock, the M_w6.1 one occurred almost at the same time as the main shock and the M_w5.0 one is an aftershock on 10 August. This provides a relatively favorable condition for seismo-ionospheric analysis of the main shock. All earthquake data obtained from the National Earthquake Information Center (NEIC) ComCat database of the U.S. Geological Survey (https://earthquake.usgs.gov/earthquakes).

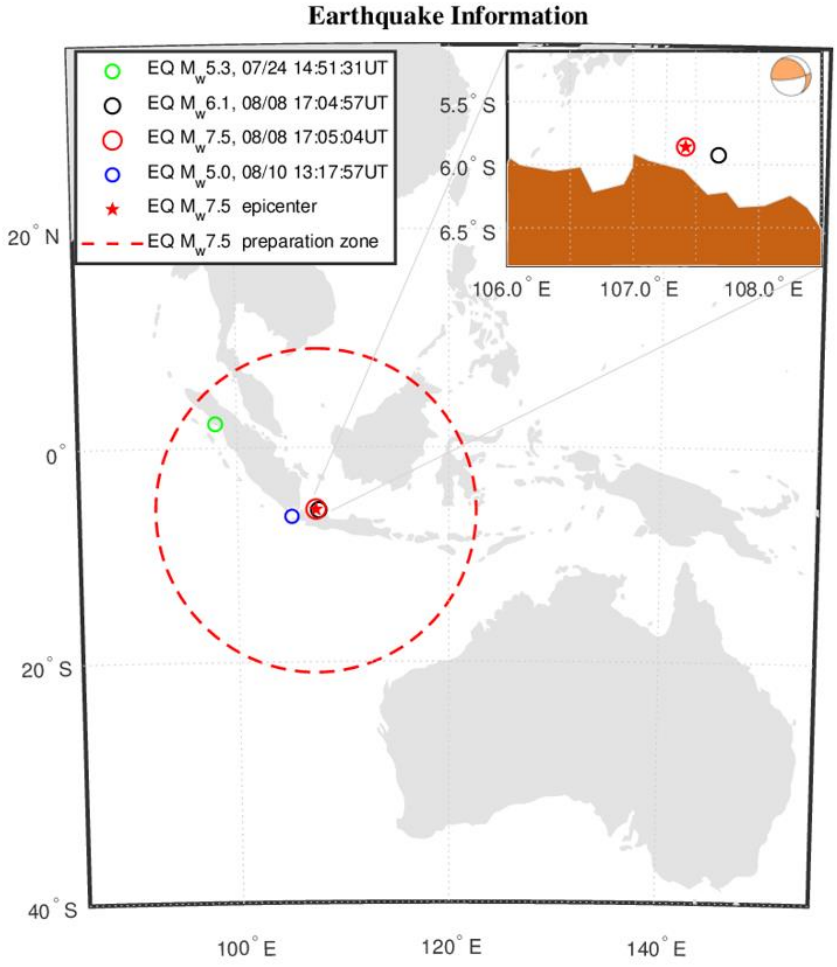

Figure 1. The 8 August 2007 M_w7.5 Jakarta-Java (5.86°S, 107.42°E) Earthquake. The red star represents the epicenter of the main shock and the red dashed circle shows the estimated earthquake preparation zone (about 1618.8 km in radius). From 24 July to 13 August 2007, there are another three $M_w \geq 5.0$ earthquakes occurred around the main shock, as shown in the legend for details. The local enlarged view in the top right corner illustrates two offshore earthquakes, i.e., EQ-M_w6.1 and EQ-M_w7.5, and the latter is an oblique-reverse type one.

3. Methodology and Observations

3.1. GIM TEC Temporal Anomalies

To detect the temporal anomalies over the epicenter of M_w7.5 Jakarta-Java earthquake, we examined GPS TEC to confirm the anomalies within 15 days before and 5 days after the main shock. TEC anomalies were detected by implementing confidence bounds of the median and associated inter-quartile ranges. Meanwhile, the bounds should be proportional to the earthquake magnitude. Here a factor of 2.0 was set for the inter-quartile range value. The confidence bounds before and after the main shock are obtained from the median and inter-quartile range of reference data of 30 days before each observed day (i.e., 30-day running) using the below equation (1-2) [8,18].

$$TEC_{UB} = MED_{30} + 2.0 \cdot IQR \quad (1)$$

$$TEC_{LB} = MED_{30} - 2.0 \cdot IQR \quad (2)$$

where TEC_{UB}, TEC_{LB}, MED_{30} and IQR are the upper and lower bounds, median and inter-quartile range calculated by 30-day running TEC values, respectively.

In this paper, we computed the TEC values over the epicenter by using a linear interpolation of four data points nearest the epicenter. Deviations in TEC, namely δ_{TEC},

are defined in equation (3) as the differences between observed TEC and confidence bounds.

$$\delta_{TEC} = \begin{cases} TEC_{observe} - TEC_{UB} & (>0;\ \text{when } TEC_{observe} > TEC_{UB}) \\ 0 & (\text{when } TEC_{observe} = TEC_{UB} \text{ or } TEC_{LB}) \\ TEC_{observe} - TEC_{LB} & (<0;\ \text{when } TEC_{observe} < TEC_{LB}) \end{cases} \quad (3)$$

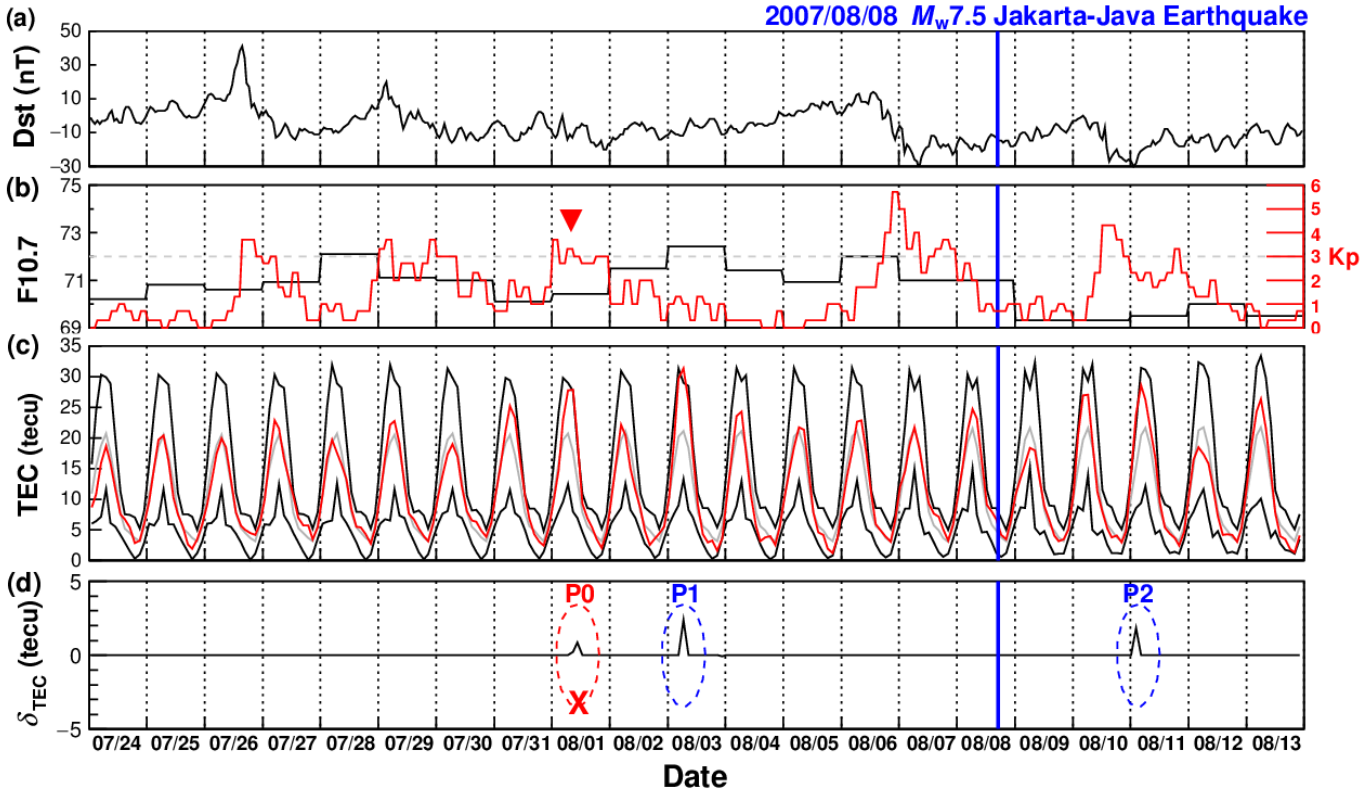

Figure 2. The ionospheric TEC temporal (from 24 July to 13 August 2007) analysis for the M_w7.5 Jakarta-Java earthquake. Subpanel (a) and (b) represent the Dst, Kp and F10.7 indices. The gray dash line indicates the Kp index equals to 3.0. Subpanel (c) shows the observed TEC value (red), 30-day running median value (gray) and the upper-lower bound (black) using the method [18]. Three periods of TEC temporal anomalies (P0-P2 illustrating with elliptic curves) were filtered out and shown in Subpanel (d). The period P0 (red elliptic curve with cross) was contaminated by magnetic storm activity indicated by the red inverted triangle in Subpanel (b). The blue vertical lines point to the moment that the main shock happened.

To interpret the ionospheric anomalies over the epicenter, we examined GPS TEC to confirm the anomalies within 15 days before and 5 days after the main shock along with the confidence bounds, as shown in Figure 2c. Similarly, the δ_{TEC} values showed abnormal feature of daily TEC. According to equation (3), three significant anomaly signals were automatically filtered out, namely period P0-P2 illustrated in Figure 2d. It was worth noting that there are abnormal TEC enhancements during period P1 (06-08 UT on 3 August, exceeding the upper bound by +8.29%) and P2 (00-02 UT on 11 August, exceeding the upper bound by +8.27%). This was consistent with the previous results that the ionospheric TEC anomalies can occur a few days before and after strong earthquake [18,63-65]. However, the signal P0 (08-12 UT on 1 August) was contaminated by magnetic storm activity and should be excluded if a stringent condition (F10.7 < 100 sfu, Dst > -30 nT and Kp < 3.0) was set for considering the potential impact of solar and geomagnetic activities. Furthermore, this affection for period P0 can also be confirmed by the results (for details

please see the supplementary materials Figure S1 and S2) with following TEC-spatial-anomaly analysis in subsection 3.2.

3.2. TEC Spatial Anomalies

In order to confirm the anomalous signals above mentioned, we conducted a spatial analysis to check if the GIM TECs simultaneously perturb over the epicenter. Figure 3 and 4 show the GIM TECs LLT map for each anomalous period. The medians of the GIM TECs, as the background values, were computed with the data during the periods of day 1-30 before the observe ones. Then the GIM extreme differences ($|\delta_{TEC}| > 0$) between the observe TEC and the associated 30-day running median one was obtained. As shown in Figure 3d and 4d, the GIM TECs over the Jakarta-Java earthquake epicenter drastically enhance up to ~ +31.52% during period P1 and ~ +13.85% during period P2, respectively. Furthermore, in order to exclude the local time and/or EIA (i.e., equatorial ionization anomaly) effects for the spatial analysis conducted above, the sequence of GIMs for the corresponding global fixed local times of anomalous periods are also examined. As shown in Figure 3h and 4h, consistent with the above TEC enhancements at the universal time, the corresponding extreme enhancements (up to ~ +31.52% during period P1 and ~ +16.91% during period P2, respectively) during the global fixed local times are also mainly located around the epicenter. Meanwhile, these enhancements are also observed near to the magnetically conjugated region of the epicenter. It is worth noting that there is a few regional background pollution of the deviations of TEC (δ_{TEC}) during period P2 (please see Figure 4c and 4g for details) probably due to geomagnetic activity ($Kp > 4.0$) the day before, i.e., on 10 August.

Therefore, the spatial anomalies simultaneously and distinctly appear during the two anomalous periods around the epicenter of Jakarta-Java earthquake and its magnetically conjugated region.

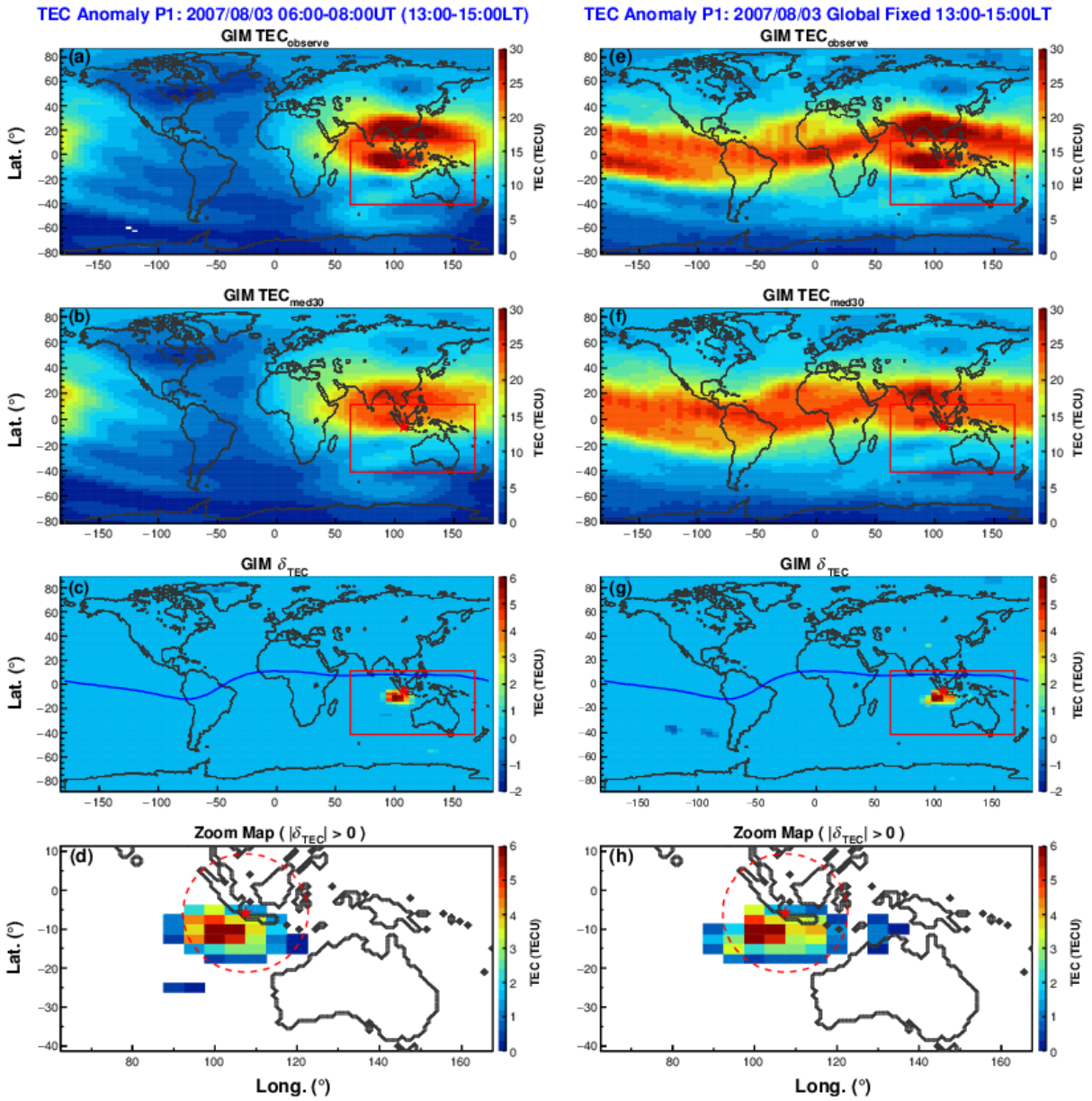

Figure 3. The spatial deviations in GIM TEC during the temporal anomalies period P1. Subpanel (a and e), (b and f) and (c and g) represent the observe GIM TEC, the 30-day running median one and the deviations of TEC (δ_{TEC}) during period P1 universal time and the global fixed local time, respectively. Subpanel (d and h) respectively represent the spatial extreme TEC anomalies ($|\delta_{TEC}| > 0$) with map zooming near the epicenter as marked with the red square in subpanel (c and g). The blue curves, red stars and dashed circles indicate the magnetic equator, the epicenter and the estimated earthquake preparation zone, respectively.

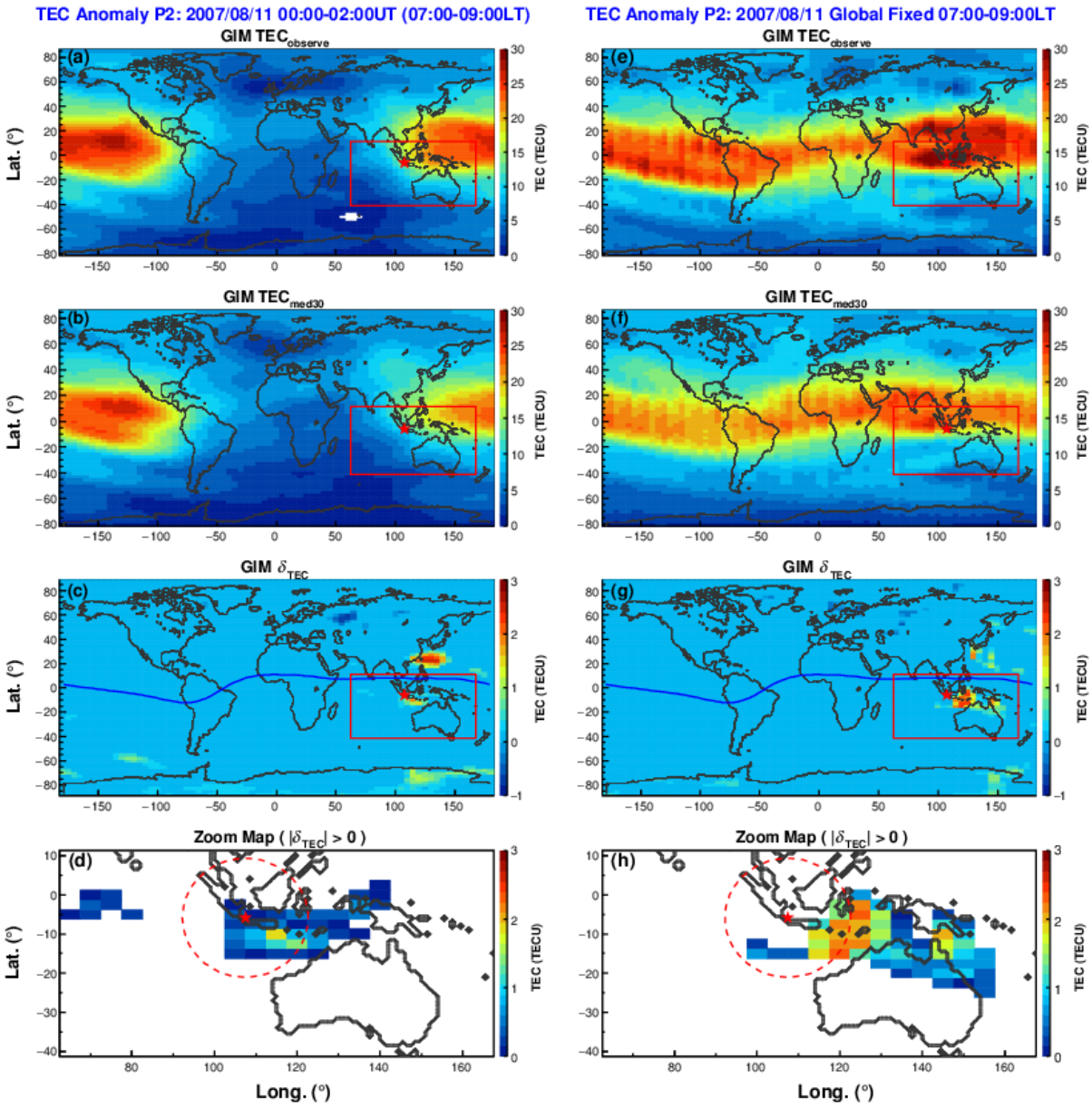

Figure 4. The spatial deviations in GIM TEC during the temporal anomalies period P2. Subpanel (a and e), (b and f) and (c and g) represent the observe GIM TEC, the 30-day running median one and the deviations of TEC (δ_{TEC}) during period P2 universal time and the global fixed local time, respectively. Subpanel (d and h) respectively represent the spatial extreme TEC anomalies ($|\delta_{TEC}| > 0$) with map zooming near the epicenter as marked with the red square in subpanel (c and g). The blue curves, red stars and dashed circles indicate the magnetic equator, the epicenter and the estimated earthquake preparation zone, respectively.

3.3. Ionospheric Plasma Anomalies

As described above, the GIM TEC anomalies extracted from GPS was analyzed during 15 days before to 5 days after the main shock. In order to further confirm ionospheric anomalies over the epicenter, a cross-validation analysis was also performed by using the data from the DEMETER satellite. Usually, the seismic-related anomalies observed by low-Earth orbit satellites deviate from the epicenter [66]. Similar to the methods described in subsection 3.1, the undisturbed reference values (the medians, upper and lower confidence bounds) were calculated with the data recorded by instruments ISL and IAP onboard DEMETER above the earthquake preparation zone. Figure 5a illustrates the time

intervals when DEMETER satellite passing above the preparation zone in the daytime from 24 July to 13 August 2007. As shown in Figure 5b and 5c, both electron (Ne) and total ion densities (Ni) increase significantly and reach their maximum values of the study periods (+3.24% for Ni on 3 August, +10.03% for Ne and +0.95% for Ni on 11 August beyond the upper bound, respectively). Besides, the main ion component O^+ density (N_{O^+}) have a clear increasing trend (as seen in Figure 5d).

Also, it should be noted that the plasma parameters reach the extremum values during periods in the daytime (i.e. 10:18:25-10:00:29 LT on 3 August along the semi-orbit 16476_0 and 10:18:10-10:00:13 LT on 11 August along the semi-orbit 16593_0) when satellite passing over the earthquake preparation zone in two down-going semi-orbits. This is also consistent well with the fact that the GIM TEC enhancements observed at the same daytime periods. However, the DEMETER satellite also passed through the earthquake preparation zone during the nighttime, but no similar variations ware found.

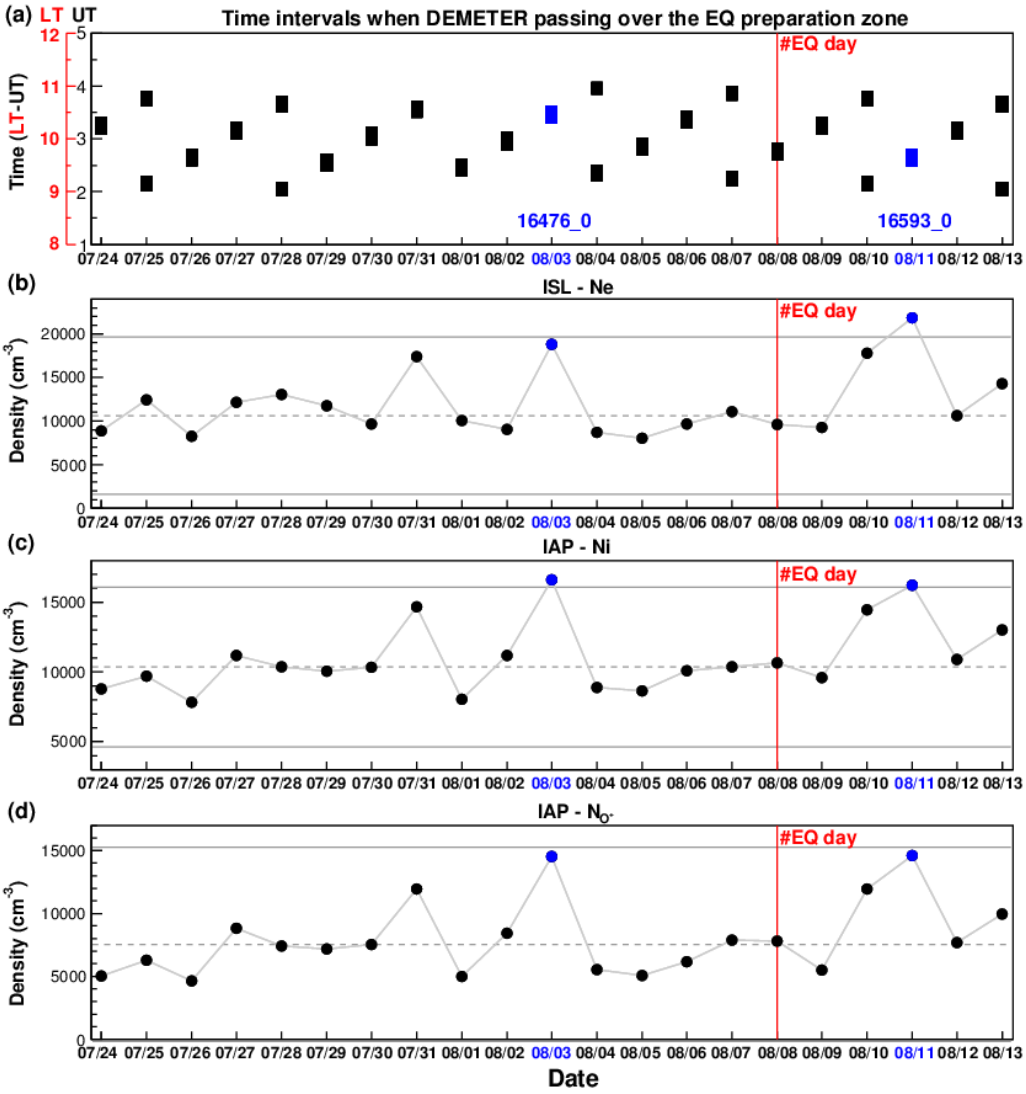

Figure 5. The plasma features above the epicenter. Subpanel (a) indicates the time intervals when satellite DEMETER passing over the EQ preparation zone from 24 July to 13 August 2007, i.e., 15 days before to 5 days after the main shock. The electron density (b), ion density (c) and O^+ density (d) detected by DEMETER during the above time intervals, respectively. The gray dash and straight lines respectively represent the medians, the lower and upper confidence bounds of plasma parameters. The blue dots indicate the values detected in 3 August and 11 August with extreme anomalies. The red vertical lines indicate the earthquake day.

4. Discussion

4.1. Possible natural and artificial electromagnetic background

In order to identify the seismo-ionospheric anomalies it is essential to assess the background due to natural non-seismic (such as atmospheric thunderstorms, volcanic eruptions and hurricane, etc.) or artificial (such as communications VLF transmitters and power line harmonic radiation, etc.) sources of electromagnetic emissions. Even so, the solar wind can also affect the dynamics of the magnetosphere on a large scale, and the solar and geomagnetic conditions have been examined in subsection 3.1.

4.1.1. Natural Non-seismic Sources

Lightning are the main source of electromagnetic noise in the ionosphere, where they generate emissions from ELF up to VHF although most of the energy is concentrated in the VLF band. Previous works have confirmed that powerful thunderstorm activities are able to perturb the ionosphere, including the enhancement of electron and ion (mainly O^+) concentrations [67-70].

In this work, the power spectrum of the ELF magnetic field and VLF electric field were checked when DEMETER was passing over the epicenter. It should be noted that data of magnetic field below ~200 Hz exist strong background noises due to the signals from payload DEMETER/IMSC can be contaminated by parasitic signals or other sources of electromagnetic interference [71,72]. In the Figure 6a and 6b, the spectrograms display vertical lines which are the whistlers due to the thunderstorm activities. Besides, the DEMETER observations (Figure 6c and 6d) seem to have similar ELF spectra to low-altitude hiss waves that are commonly found in the ionosphere [73,74]. This electromagnetic whistler-mode hiss may leak out of the plasmasphere at higher altitude and then turn into low-altitude hiss in the ionosphere, which will play important roles for radiation belt loss and acceleration. For the event analyzed here, the ELF waves have weaker intensity due to at dayside (about 10:00 LT). As the analysis duration is from July to August, it is summer close to the equator, and it is noteworthy that such significant plasma disturbances are not detected during other periods over the epicenter, as seen in Figure 5, even in the similar electromagnetic emission background. It can be illustrated that along the semi-orbit 16593_0 where the electromagnetic background is relatively obvious but not very strong, however, the plasma disturbances due to electromagnetic factor cannot be completely excluded.

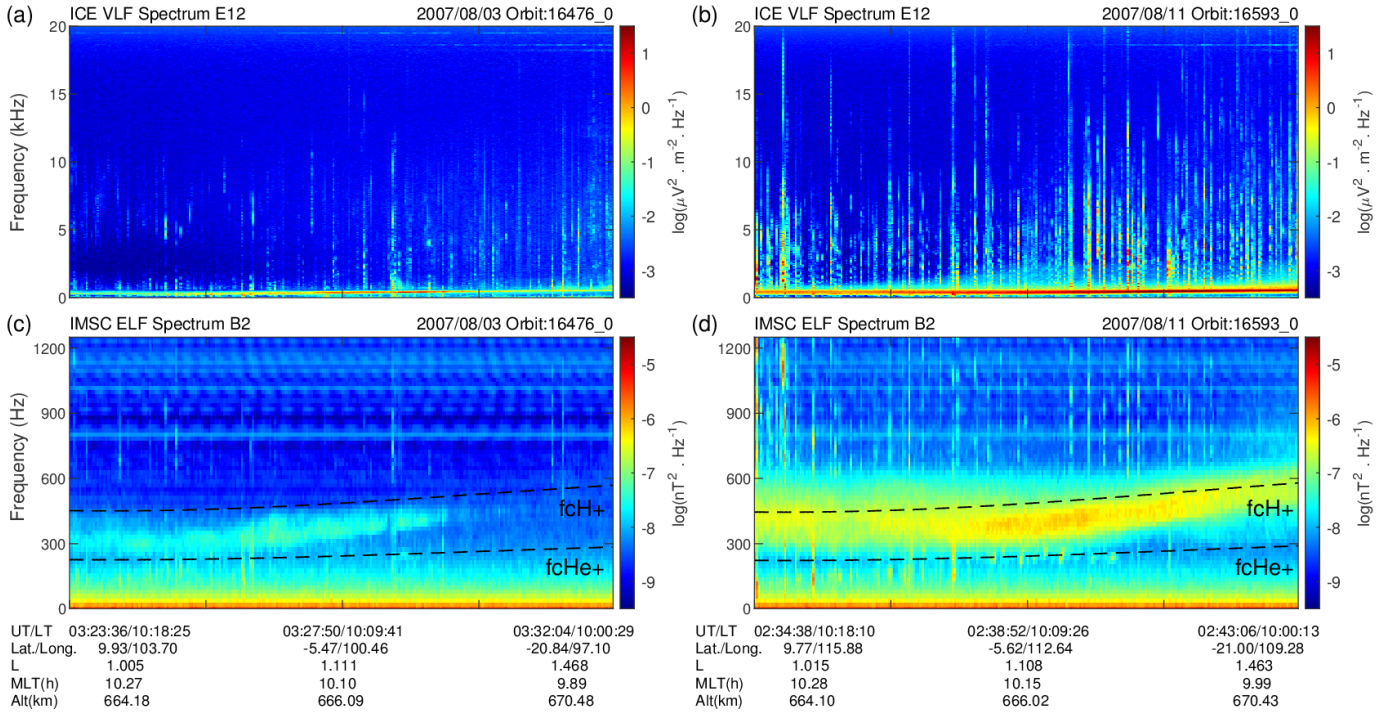

Figure 6. The VLF electric spectrum (E12 - frequency: 0-20 kHz) and ELF magnetic spectrum (B2 – frequency: 0-1250 Hz) respectively provided by the ICE and IMSC instrument aboard DEMETER: (a and c) semi-orbit 16476_0 and (b and d) semi-orbit 16593_0. The intensity is color-coded according to the color scale on the right. Also ion (H^+ and He^+) gyrofrequencies (fcH^+ and $fcHe^+$) are over-plotted in magnetic spectra (c and d).

4.1.2. The powerful Ground-Based VLF Transmitters

Many studies have shown that powerful ground-based communications VLF transmitters around tens of kHz frequency band can trigger new waves, ionospheric heating, wave-particle interactions, and particle precipitation via the cyclotron resonance [75-80]. Due to the power of the artificial signals can overwhelm the natural and faint emissions possibly associated to earthquakes, frequencies range around the band of the known VLF transmitters need to be considered in the analysis of seismo-associated disturbance.

Table 1. The information of four VLF transmitters in the Asian sector

No.	NAME	LAT.	LONG.	FREQ. (kHz)
1	UBE	52.90	158.55	16.20
2	NTS	-38.48	146.93	18.60
3	NWC	-21.82	114.17	19.80
4	NDT	32.08	130.83	22.20

Figure 7 displays the average power distribution measured by the ICE instrument aboard DEMETER during the nighttime and daytime, respectively. In the Asian sector (70°E-160°E), four main transmitters are long-running: UBE (at 16.20 kHz) and NDT (at 22.20 kHz) in the northern hemisphere, and NWC (at 19.8 kHz) and NTS (at 18.60 kHz) in the southern hemisphere. Table 1 provides the information of above four VLF transmitters. Among these VLF transmitters, the Naval Communication Station Harold E. Holt ("NWC") in Western Australia is the most effective one. When NWC is on, its average power is about three orders of magnitude higher than the other three and the distribution of VLF waves in the vicinity of Australia and in the conjugate hemisphere. However, the emission is significantly reduced when the NWC transmitter is off, i.e., from July 2007 to

January 2008. Furthermore, comparing to the nighttime, the daytime power is much lower because the stronger absorption in the ionosphere during the daytime (please see Figure 7b for details). In our case, the data analysis cycle (from 24 July to 13 August 2007) is coinciding with the off-time of NWC transmitter and the two anomaly periods, i.e., P1 and P2, appear in the daytime. In view of this, we have reason to believe that the seismo-ionospheric anomaly here is minimally influenced by the known man-made VLF transmitters.

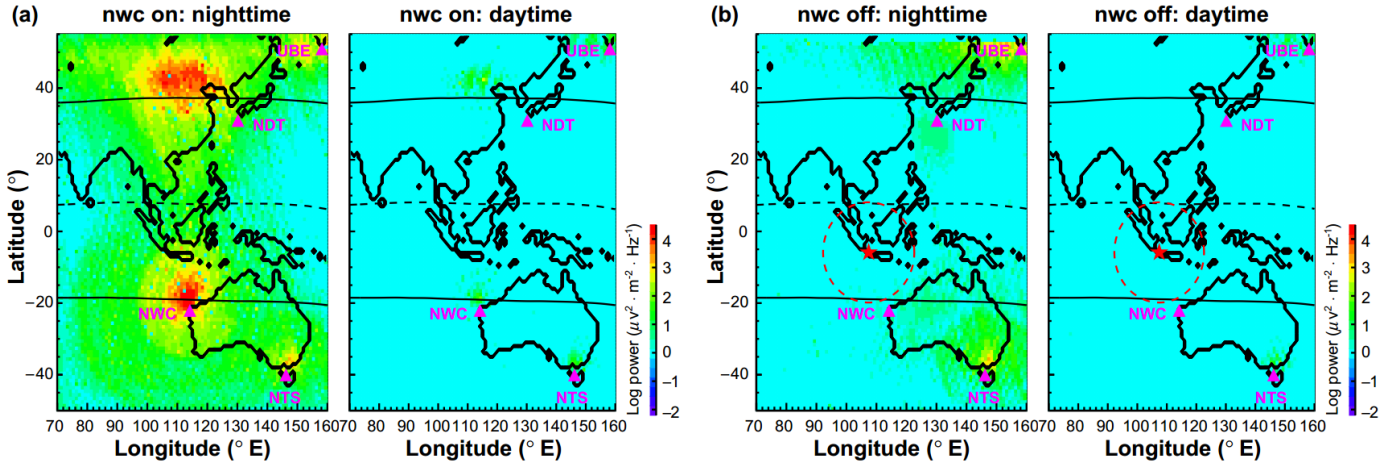

Figure 7. The average VLF power spectral density measured by the ICE instrument aboard DEMETER in the Asian sector (70°E-160°E). When NWC is (a) ON (from July 2006 to January 2007) and (b) OFF (from July 2007 to January 2008): the distribution of average power spectral density at each VLF transmitting frequency during the nighttime and daytime, respectively. The geolocations of four artificial VLF transmitters (i.e., UBE, NTS, NWC and NDT) marked with magenta solid triangles. The black solid carves indicate the L = 1.4 contours at the satellite altitude and the black dashed ones show the magnetic equator. The red stars indicate the epicenter of Jakarta-Java earthquake. The red dashed circles indicate the estimated earthquake preparation zone.

4.2. Possible physical mechanism

Although the possible earthquake precursors (on long, middle or short temporal scale) observed on ground (or under the sea) or in space have been reported in many previous studies, the possible pre-earthquake phenomena as well as the coupling between the lithosphere, atmosphere and ionosphere are still disputed. As it is difficult to detail a debate, here we discuss only the most likely or reliable mechanism for the ionospheric pre-seismic fluctuations of large undersea earthquake. Considering the focal depth of large undersea earthquake and its energy loss transmitted to the seafloor, the hypothesis that the lithosphere-atmosphere-ionosphere coupling could be due to the atmosphereic processes including infrasonic acoustic waves (IAWs) or acoustic (AWs) and acoustic gravity waves (AGWs) [28,29,51-57,81] seems more reasonable, despite it will suffer of the difficulty to some extent.

The infrasonic acoustic waves or acoustic and acoustic gravity waves close to the Earth's surface can be generated by ground vibrations (such as the low-frequency crustal vibrations) before earthquakes [28,29,82-88]. Even if some aspects of the evolution of this kind of preseismic vibrations still unclear, such as their temporal and spatial scales. Then, seismically induced waves, excited at water-air interfaces, will propagate to the upper layers of atmosphere and generate fluctuations of densities, temperatures and the ionospheric plasma (Figure 8a). Recently, Inchin et al. (2020 and 2021) have successfully reproduced the ionospheric responses to atmospheric infrasonic/acoustic and gravity waves driven by the large earthquakes. Furthermore, the amplitude of the vertical crustal dis-

placements is considered to be a very important factor for the generation of sesimo-ionospheric perturbations [89,90] and the Jakarta-Java earthquake is an oblique-reverse case and characterized by significant vertical crustal motion [91].

Even so, due to the variability or uncertainty of the temporal and spatial scales of the ionospheric pre-seismic fluctuations, it is still difficult to interpret them by only one mechanism. On this basis, some other promising hypothesis have also been proposed, especially the gases (mainly radon) and aerosol release during both in land and undersea earthquakes. Possible radon emission during the earthquake preparation phase can well explain the model of atmospheric thermal anomalies which could generate atmospheric oscillations and then trigger acoustic gravity waves [48,92-101], as shown schematically in Figure 8b. Meanwhile, the increased aerosol release in seismic regions during the earthquake preparation phase could also spread into the atmosphere and then affect the electromagnetic environment [43,44,46-48]. Up to now, the IAWs or AWs/AGWs are thought to play a key role in the LAI coupling process.

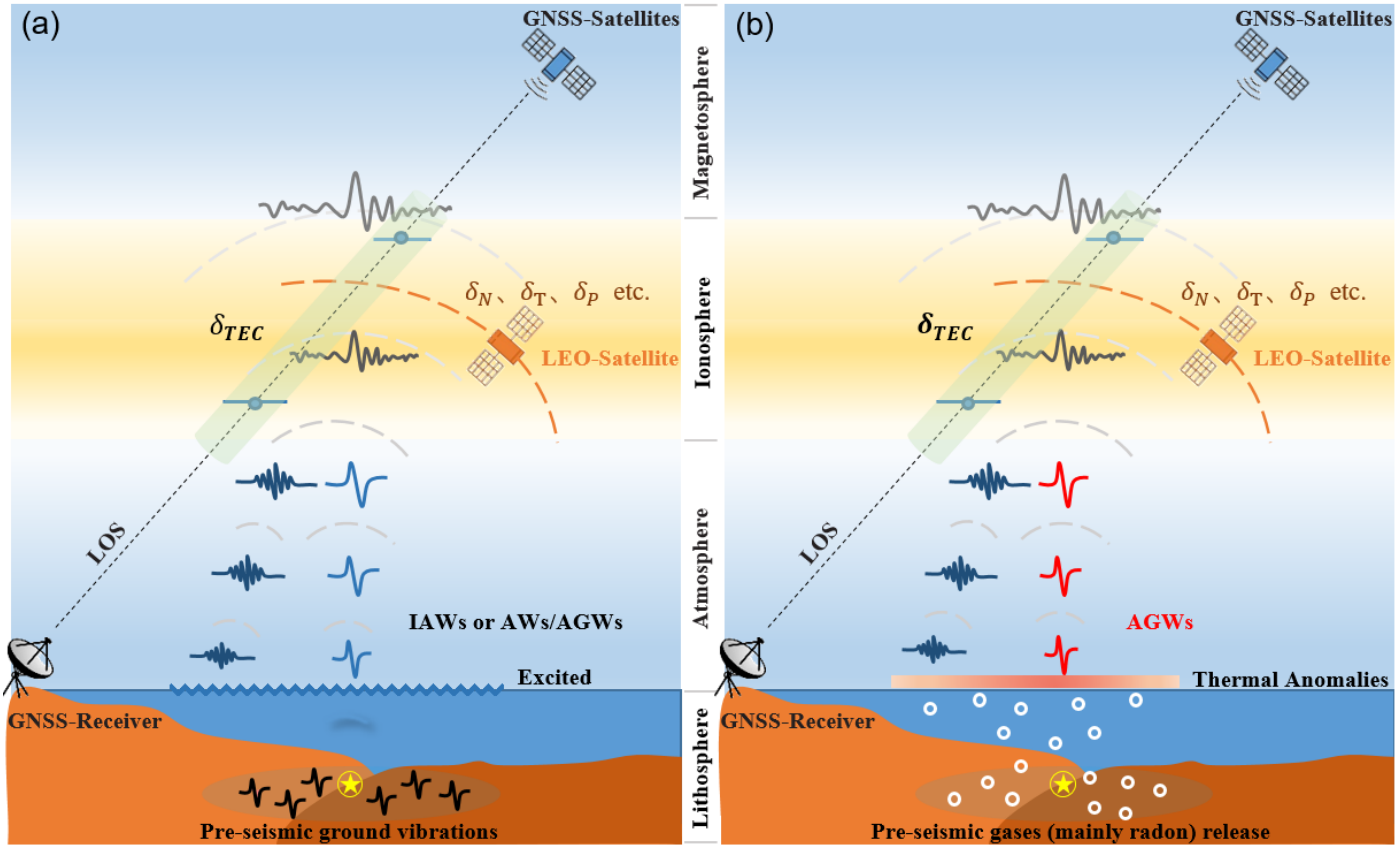

Figure 8. Schematic representation of the undersea earthquake-atmosphere-ionosphere coupling. (a) Induced IAWs or AWs/AGWs due to pre-seismic ground vibrations and excited at water-air interfaces, (b) Possible radon emission during the earthquake preparation phase contributes to atmospheric thermal anomalies which could generate atmospheric oscillations and then trigger acoustic gravity waves. Then waves will propagate to the upper layers of atmosphere and generate ionospheric disturbances, such as fluctuation in TEC (δ_{TEC}) detected by GNSS and densities (δ_N), temperatures (δ_T) the ionospheric plasma (δ_P) detected by low-earth-orbit (LEO) satellites. TEC represents the total electron content along line-of-sight (LOS) between GNSS satellite and receiver. GNSS, Global Navigation Satellite System.

5. Conclusions

Nowadays, earthquake forecasting is far from being reached and the debated about ionospheric earthquake precursors is still open. However, the set of observed precursors is varied and remarkable, it prompts us to explain the underlying physical mechanism for

coupling the lithosphere with lower and upper layers of the atmosphere up to the ionosphere. In this framework, we focused on a special (undersea and deep-focus) earthquake in detail in order to identify the possible connection between large undersea seismic activities and ionospheric anomalies.

We highlight the following general conclusions as well:

1. In order to identify the correlation between the earthquakes and ionospheric disturbances, the efforts were made to distinguish seismo-associated signals from large electromagnetic noise due to natural non-seismic sources, artificial signals and geomagnetic activities. Nevertheless, the difficulties of this work should be recognized and approached with caution.
2. The significant TEC spatial and temporal anomalies were detected during period P1 and P2 over the epicenter of 2007 M_w7.5 Jakarta-Java earthquake, and they coincide well with the striking plasma anomalies in the ionosphere in-situ observed by the LEO satellite. The localization and synchronization of the disturbances during the earthquake suggest that these ionospheric anomalies are highly related to this undersea earthquake. However, the background, mainly due to geomagnetic and thunderstorm activities and local low-altitude hiss, is a bit complicated during period P2.
3. For great undersea earthquakes, considering their focal depth and energy loss transmitted to the seafloor, seismically induced IAWs or AWs/AGWs due to pre-seismic ground vibrations or AWGs result from radon emission during the earthquake preparation phase could be responsible of the coupling between undersea earthquakes and ionospheric disturbances.

More recently, IAWs or AWs/AGWs are thought to play an important role in the lithosphere-atmosphere-ionosphere coupling process and further support to this hypothesis should be provided. However, an integrated system that can monitor this coupling process between the ground and space is insufficient. Fortunately, the high-density geophysical arrays for monitoring vibrations and perturbations in the LAI (called MVP–LAI system) were established in China in 2021 [102]. It will provide an excellent opportunity for monitoring vibrations and perturbations in the vertical direction and promote the understanding the physical mechanism of LAI coupling.

Supplementary Materials: The following supporting information can be downloaded at: www.mdpi.com/xxx/s1, Figure S1 and S2: The spatial deviations in GIM TEC during the temporal anomalies period P0.

Author Contributions: Conceptualization, D.T.; methodology, D.T.; software, D.T. and G.W.; validation, D.T.; formal analysis, D.T.; investigation, D.T., G.W., J.Z. and Y.W.; resources, D.T.; data curation, D.T., G.W., J.Z. and Y.W.; writing—original draft preparation, D.T.; writing—review and editing, D.T.; visualization, D.T.; supervision, J.C., R.B. and Z.Z.; project administration, D.T.; funding acquisition, D.T. All authors have read and agreed to the published version of the manuscript.

Funding: This research was funded by NATIONAL NATURAL SCIENCE FOUNDATION OF CHINA (NSFC), grant number 42004137.

Data Availability Statement: The earthquake data are available at https://earthquake.usgs.gov/earthquakes. GPS-TEC data are available at https://cdaweb.gsfc.nasa.gov/sp_phys/ and DEMETER data are accessible from https://cdpp-archive.cnes.fr.

Acknowledgments: We acknowledge use of GPS TEC data provided by the Jet Propulsion Lab (JPL) and DEMETER data available from the CDPP server (https://sipad-cdpp.cnes.fr/). We also thank the National Earthquake Information Center (NEIC) ComCat database of the US Geological Survey for providing available earthquake data. This work was supported by National Natural Science Foundation of China (grant number 42004137).

Conflicts of Interest: The authors declare no conflict of interest.

References

1. Jones, L.; Molnar, P. Frequency of foreshocks. *Nature* **1976**, *262*, 677-679, doi:10.1038/262677a0.
2. Sornette, A.; Sornette, D. Self-organized criticality and earthquakes. *Europhysics Letters* **1989**, *9*, 197–202, doi:10.1209/0295-5075/9/3/002.
3. Parrot, M. Statistical study of ELF/VLF emissions recorded by a low-altitude satellite during seismic events. *Journal of Geophysical Research: Space Physics* **1994**, *99*, 23339-23347, doi:10.1029/94ja02072.
4. Hayakawa, M.; Kawate, R.; Molchanov, O.A.; Yumoto, K. Results of ultra-low-frequency magnetic field measurements during the Guam earthquake of 8 August 1993. *Geophys Res Lett* **1996**, *23*, 241-244, doi:10.1029/95gl02863.
5. Tramutoli, V. Robust AVHRR Techniques (RAT) for environmental monitoring: theory and applications. In Proceedings of the Earth Surface Remote Sensing II, 1998; pp. 101-113.
6. Gokhberg, M.B.; Shalimov, S.L. Lithosphere-ionosphere relation and its modeling. *Russian Journal of Earth Sciences* **2000**, *2*, 95–108, doi:10.2205/2000ES000032.
7. Sgrigna, V.; Malvezzi, V. Preseismic creep strains revealed by ground tilt measurements in central Italy on the occasion of the 1997 Umbria-Marche Apennines earthquake sequence. *Pure Appl Geophys* **2003**, *160*, 1493-1515, doi:10.1007/s00024-003-2357-5.
8. Liu, J.Y.; Chuo, Y.J.; Shan, S.J.; Tsai, Y.B.; Chen, Y.I.; Pulinets, S.A.; Yu, S.B. Pre-earthquake ionospheric anomalies registered by continuous GPS TEC measurements. *Ann Geophys-Germany* **2004**, *22*, 1585-1593, doi:10.5194/angeo-22-1585-2004.
9. Ouzounov, D.; Freund, F. Mid-infrared emission prior to strong earthquakes analyzed by remote sensing data. *Adv Space Res* **2004**, *33*, 268-273, doi:10.1016/s0273-1177(03)00486-1.
10. Tramutoli, V.; Cuomo, V.; Filizzola, C.; Pergola, N.; Pietrapertosa, C. Assessing the potential of thermal infrared satellite surveys for monitoring seismically active areas: The case of Kocaell (Izmit) earthquake, August 17, 1999. *Remote Sensing of Environment* **2005**, *96*, 409-426, doi:10.1016/j.rse.2005.04.006.
11. Sorokin, V.M.; Isaev, N.V.; Yaschenko, A.K.; Chmyrev, V.M.; Hayakawa, M. Strong DC electric field formation in the low latitude ionosphere over typhoons. *J Atmos Sol-Terr Phy* **2005**, *67*, 1269-1279, doi:10.1016/j.jastp.2005.06.014.
12. Ouzounov, D.; Liu, D.; Kang, C.; Cervone, G.; Kafatos, M.; Taylor, P. Outgoing long wave radiation variability from IR satellite data prior to major earthquakes. *Tectonophysics* **2007**, *431*, 211-220, doi:10.1016/j.tecto.2006.05.042.
13. Nemec, F.; Santolik, O.; Parrot, M.; Berthelier, J.J. Spacecraft observations of electromagnetic perturbations connected with seismic activity. *Geophys Res Lett* **2008**, *35*, L05109, doi:10.1029/2007gl032517.
14. Fidani, C.; Battiston, R. Analysis of NOAA particle data and correlations to seismic activity. *Nat Hazard Earth Sys* **2008**, *8*, 1277-1291, doi:10.5194/nhess-8-1277-2008.
15. Nemec, F.; Santolik, O.; Parrot, M. Decrease of intensity of ELF/VLF waves observed in the upper ionosphere close to earthquakes: A statistical study. *J Geophys Res-Space* **2009**, *114*, A04303, doi:10.1029/2008ja013972.
16. Nemec, F.; Santolik, O.; Parrot, M.; Rodger, C.J. Relationship between median intensities of electromagnetic emissions in the VLF range and lightning activity. *J Geophys Res-Space* **2010**, *115*, A08315, doi:10.1029/2010ja015296.
17. Liu, J.Y.; Chen, C.H.; Chen, V.I.; Yang, W.H.; Oyama, K.I.; Kuo, K.W. A statistical study of ionospheric earthquake precursors monitored by using equatorial ionization anomaly of GPS TEC in Taiwan during 2001-2007. *J Asian Earth Sci* **2010**, *39*, 76-80, doi:10.1016/j.jseaes.2010.02.012.
18. Akhoondzadeh, M.; Parrot, M.; Saradjian, M.R. Electron and ion density variations before strong earthquakes (M > 6.0) using DEMETER and GPS data. *Nat Hazard Earth Sys* **2010**, *10*, 7-18, doi:10.5194/nhess-10-7-2010.
19. Kuo, C.L.; Huba, J.D.; Joyce, G.; Lee, L.C. Ionosphere plasma bubbles and density variations induced by pre-earthquake rock currents and associated surface charges. *J Geophys Res-Space* **2011**, *116*, A10317, doi:10.1029/2011ja016628.

20. Battiston, R.; Vitale, V. First evidence for correlations between electron fluxes measured by NOAA-POES satellites and large seismic events. *Nuclear Physics B-Proceedings Supplements* **2013**, *243-244*, 249-257, doi:10.1016/j.nuclphysbps.2013.09.002.
21. Pisa, D.; Nemec, F.; Santolik, O.; Parrot, M.; Rycroft, M. Additional attenuation of natural VLF electromagnetic waves observed by the DEMETER spacecraft resulting from preseismic activity. *J Geophys Res-Space* **2013**, *118*, 5286-5295, doi:10.1002/jgra.50469.
22. Kuo, C.L.; Lee, L.C.; Huba, J.D. An improved coupling model for the lithosphere-atmosphere-ionosphere system. *J Geophys Res-Space* **2014**, *119*, 3189-3205, doi:10.1002/2013ja019392.
23. De Santis, A. Geosystemics, Entropy and Criticality of Earthquakes: A Vision of Our Planet and a Key of Access. In Proceedings of the Nonlinear Phenomena in Complex Systems: From Nano to Macro Scale, 2014; pp. 3-20.
24. Lu, X.; Meng, Q.Y.; Gu, X.F.; Zhang, X.D.; Xie, T.; Geng, F. Thermal infrared anomalies associated with multi-year earthquakes in the Tibet region based on China's FY-2E satellite data. *Adv Space Res* **2016**, *58*, 989-1001, doi:10.1016/j.asr.2016.05.038.
25. Tao, D.; Cao, J.; Battiston, R.; Li, L.; Ma, Y.; Liu, W.; Zhima, Z.; Wang, L.; Dunlop, M.W. Seismo-ionospheric anomalies in ionospheric TEC and plasma density before the 17 July 2006 M7.7 south of Java earthquake. *Ann Geophys-Germany* **2017**, *35*, 589-598, doi:10.5194/angeo-35-589-2017.
26. Ma, W.; Zhang, X.; Jun, L.; Qi, Y.; Bo, Z.; Chong, Y.; Kang, C.; Xian, L. Influences of multiple layers of air temperature differences on tidal forces and tectonic stress before, during and after the Jiujiang earthquake. *Remote Sensing of Environment* **2018**, *210*, 159-165, doi:10.1016/j.rse.2018.03.003.
27. Xiong, P.; Long, C.; Zhou, H.; Battiston, R.; Zhang, X.; Shen, X. Identification of Electromagnetic Pre-Earthquake Perturbations from the DEMETER Data by Machine Learning. *Remote Sensing* **2020**, *12*, 3643, doi:10.3390/rs12213643.
28. Inchin, P.A.; Snively, J.B.; Zettergren, M.D.; Komjathy, A.; Verkhoglyadova, O.P.; Ram, S.T. Modeling of Ionospheric Responses to Atmospheric Acoustic and Gravity Waves Driven by the 2015 Nepal M(w)7.8 Gorkha Earthquake. *J Geophys Res-Space* **2020**, *125*, e2019JA027200, doi:10.1029/2019ja027200.
29. Inchin, P.A.; Snively, J.B.; Kaneko, Y.; Zettergren, M.D.; Komjathy, A. Inferring the Evolution of a Large Earthquake From Its Acoustic Impacts on the Ionosphere. *Agu Advances* **2021**, *2*, e2020AV000260, doi:10.1029/2020av000260.
30. Xiong, P.; Tong, L.; Zhang, K.; Shen, X.; Battiston, R.; Ouzounov, D.; Iuppa, R.; Crookes, D.; Long, C.; Zhou, H. Towards advancing the earthquake forecasting by machine learning of satellite data. *Science of the Total Environment* **2021**, *771*, 145256, doi:10.1016/j.scitotenv.2021.145256.
31. Picozza, P.; Conti, L.; Sotgiu, A. Looking for Earthquake Precursors From Space: A Critical Review. *Frontiers in Earth Science* **2021**, *9*, doi:10.3389/feart.2021.676775.
32. Conti, L.; Picozza, P.; Sotgiu, A. A Critical Review of Ground Based Observations of Earthquake Precursors. *Frontiers in Earth Science* **2021**, *9*, doi:10.3389/feart.2021.676766.
33. Zhang, X.; Wang, Y.; Boudjada, M.; Liu, J.; Magnes, W.; Zhou, Y.; Du, X. Multi-Experiment Observations of Ionospheric Disturbances as Precursory Effects of the Indonesian Ms6.9 Earthquake on August 05, 2018. *Remote Sensing* **2020**, *12*, 4050, doi:10.3390/rs12244050.
34. Heki, K.; Ping, J.S. Directivity and apparent velocity of the coseismic ionospheric disturbances observed with a dense GPS array. *Earth and Planetary Science Letters* **2005**, *236*, 845-855, doi:10.1016/j.epsl.2005.06.010.
35. Heki, K.; Otsuka, Y.; Choosakul, N.; Hemmakorn, N.; Komolmis, T.; Maruyama, T. Detection of ruptures of Andaman fault segments in the 2004 great Sumatra earthquake with coseismic ionospheric disturbances. *J Geophys Res-Sol Ea* **2006**, *111*, B09313, doi:10.1029/2005jb004202.
36. Liu, J.Y.; Tsai, H.F.; Lin, C.H.; Kamogawa, M.; Chen, Y.I.; Lin, C.H.; Huang, B.S.; Yu, S.B.; Yeh, Y.H. Coseismic ionospheric disturbances triggered by the Chi-Chi earthquake. *J Geophys Res-Space* **2010**, *115*, A08303, doi:10.1029/2009ja014943.

37. Matsuo, K.; Heki, K. Coseismic gravity changes of the 2011 Tohoku-Oki earthquake from satellite gravimetry. *Geophys Res Lett* **2011**, *38*, L00G12, doi:10.1029/2011gl049018.
38. Song, Q.; Ding, F.; Yu, T.; Wan, W.; Ning, B.; Liu, L.; Zhao, B. GPS detection of the coseismic ionospheric disturbances following the 12 May 2008 M7.9 Wenchuan earthquake in China. *Sci China Earth Sci* **2015**, *58*, 151-158, doi:10.1007/s11430-014-5000-7.
39. Cahyadi, M.N.; Heki, K. Coseismic ionospheric disturbance of the large strike-slip earthquakes in North Sumatra in 2012: M-w dependence of the disturbance amplitudes. *Geophys J Int* **2015**, *200*, 116-129, doi:10.1093/gji/ggu343.
40. Gao, Y.; Harris, J.M.; Wen, J.; Huang, Y.; Twardzik, C.; Chen, X.; Hu, H. Modeling of the coseismic electromagnetic fields observed during the 2004 M-w 6.0 Parkfield earthquake. *Geophys Res Lett* **2016**, *43*, 620-627, doi:10.1002/2015gl067183.
41. Ram, S.T.; Sunil, P.S.; Kumar, M.R.; Su, S.Y.; Tsai, L.C.; Liu, C.H. Coseismic Traveling Ionospheric Disturbances during the M-w 7.8 Gorkha, Nepal, Earthquake on 25 April 2015 From Ground and Spaceborne Observations. *J Geophys Res-Space* **2017**, *122*, 10669-10685, doi:10.1002/2017ja023860.
42. Liu, H.; Zhang, K.; Imtiaz, N.; Song, Q.; Zhang, Y. Relating Far-Field Coseismic Ionospheric Disturbances to Geological Structures. *J Geophys Res-Space* **2021**, *126*, e2021JA029209, doi:10.1029/2021ja029209.
43. Harper, W.R. The generation of static charge. *Advances in Physics* **1957**, *6*, 365-417, doi:10.1080/00018735700101396.
44. Blanchard, D.C. The electrification of the atmosphere by particles from bubbles in the sea. *Progress in oceanography* **1963**, *1*, 73–202, doi:10.1016/0079-6611(63)90004-1.
45. King, C.Y. Gas geochemistry applied to earthquake prediction: An overview. *Journal of Geophysical Research: Solid Earth* **1986**, *91*, 12269-12281, doi:10.1029/jb091ib12p12269.
46. Zavarsky, A.; Booge, D.; Fiehn, A.; Kruger, K.; Atlas, E.; Marandino, C. The Influence of Air-Sea Fluxes on Atmospheric Aerosols During the Summer Monsoon Over the Tropical Indian Ocean. *Geophys Res Lett* **2018**, *45*, 418-426, doi:10.1002/2017gl076410.
47. Revell, L.E.; Kremser, S.; Hartery, S.; Harvey, M.; Mulcahy, J.P.; Williams, J.; Morgenstern, O.; McDonald, A.J.; Varma, V.; Bird, L.; et al. The sensitivity of Southern Ocean aerosols and cloud microphysics to sea spray and sulfate aerosol production in the HadGEM3-GA7.1 chemistry-climate model. *Atmospheric Chemistry and Physics* **2019**, *19*, 15447-15466, doi:10.5194/acp-19-15447-2019.
48. Sorokin, V.M.; Chmyrev, V.M.; Hayakawa, M. A Review on Electrodynamic Influence of Atmospheric Processes to the Ionosphere. *Open Journal of Earthquake Research* **2020**, *9*, 113-141, doi:10.4236/ojer.2020.92008.
49. Blanc, E. Observations in the upper atmosphere of infrasonic waves from natural or artificial sources-A summary. *Ann Geophys-Germany* **1985**, *3*, 673-687.
50. Hargreaves, J.K. *The solar-terrestrial environment: an introduction to geospace-the science of the terrestrial upper atmosphere, ionosphere, and magnetosphere*; Cambridge University Press: New York, 1992.
51. Kaladze, T.D.; Pokhotelov, O.A.; Shah, H.A.; Khan, M.I.; Stenflo, L. Acoustic-gravity waves in the Earth's ionosphere. *J Atmos Sol-Terr Phy* **2008**, *70*, 1607-1616, doi:10.1016/j.jastp.2008.06.009.
52. Godin, O.A. Acoustic-gravity waves in atmospheric and oceanic waveguides. *Journal of the Acoustical Society of America* **2012**, *132*, 657-669, doi:10.1121/1.4731213.
53. Godin, O.A.; Zabotin, N.A.; Bullett, T.W. Acoustic-gravity waves in the atmosphere generated by infragravity waves in the ocean. *Earth, Planets and Space* **2015**, *67*, 47, doi:10.1186/s40623-015-0212-4.
54. Zettergren, M.D.; Snively, J.B. Ionospheric response to infrasonic-acoustic waves generated by natural hazard events. *J Geophys Res-Space* **2015**, *120*, 8002-8024, doi:10.1002/2015ja021116.
55. Kadri, U. Tsunami mitigation by resonant triad interaction with acoustic-gravity waves. *Heliyon* **2017**, *3*, e00234-e00234, doi:10.1016/j.heliyon.2017.e00234.

56. Yang, S.-S.; Asano, T.; Hayakawa, M. Abnormal Gravity Wave Activity in the Stratosphere Prior to the 2016 Kumamoto Earthquakes. *J Geophys Res-Space* **2019**, *124*, 1410-1425, doi:10.1029/2018ja026002.
57. Liu, Y.; Jin, S. Ionospheric Rayleigh Wave Disturbances Following the 2018 Alaska Earthquake from GPS Observations. *Remote Sensing* **2019**, *11*, doi:10.3390/rs11080901.
58. Parrot, M.; Benoist, D.; Berthelier, J.J.; Blecki, J.; Chapuis, Y.; Colin, F.; Elie, F.; Fergeau, P.; Lagoutte, D.; Lefeuvre, F.; et al. The magnetic field experiment IMSC and its data processing onboard DEMETER: Scientific objectives, description and first results. *Planet Space Sci* **2006**, *54*, 441-455, doi:10.1016/j.pss.2005.10.015.
59. Lebreton, J.P.; Stverak, S.; Travnicek, P.; Maksimovic, M.; Klinge, D.; Merikallio, S.; Lagoutte, D.; Poirier, B.; Blelly, P.L.; Kozacek, Z.; et al. The ISL Langmuir probe experiment processing onboard DEMETER: Scientific objectives, description and first results. *Planet Space Sci* **2006**, *54*, 472-486, doi:10.1016/j.pss.2005.10.017.
60. Berthelier, J.J.; Godefroy, M.; Leblanc, F.; Seran, E.; Peschard, D.; Gilbert, P.; Artru, J. IAP, the thermal plasma analyzer on DEMETER. *Planet Space Sci* **2006**, *54*, 487-501, doi:10.1016/j.pss.2005.10.018.
61. Berthelier, J.J.; Godefroy, M.; Leblanc, F.; Malingre, M.; Menvielle, M.; Lagoutte, D.; Brochot, J.Y.; Colin, F.; Elie, F.; Legendre, C.; et al. ICE, the electric field experiment on DEMETER. *Planet Space Sci* **2006**, *54*, 456-471, doi:10.1016/j.pss.2005.10.016.
62. Dobrovolsky, I.P.; Zubkov, S.I.; Miachkin, V.I. Estimation of the size of earthquake preparation zones. *Pure Appl Geophys* **1979**, *117*, 1025-1044, doi:10.1007/BF00876083.
63. Pulinets, S.A.; Legen'ka, A.D.; Gaivoronskaya, T.V.; Depuev, V.K. Main phenomenological features of ionospheric precursors of strong earthquakes. *J Atmos Sol-Terr Phy* **2003**, *65*, 1337-1347, doi:10.1016/j.jastp.2003.07.011.
64. Pulinets, S.; Davidenko, D. Ionospheric precursors of earthquakes and Global Electric Circuit. *Adv Space Res* **2014**, *53*, 709-723, doi:10.1016/j.asr.2013.12.035.
65. Pulinets, S.A.; Ouzounov, D.P.; Karelin, A.V.; Davidenko, D.V. Physical bases of the generation of short-term earthquake precursors: A complex model of ionization-induced geophysical processes in the lithosphere-atmosphere-ionosphere-magnetosphere system. *Geomagn Aeronomy+* **2015**, *55*, 521-538, doi:10.1134/s0016793215040131.
66. Zhima, Z.; Cao, J.; Liu, W.; Fu, H.; Wang, T.; Zhang, X.; Shen, X. Storm time evolution of ELF/VLF waves observed by DEMETER satellite. *J Geophys Res-Space* **2014**, *119*, 2612-2622, doi:10.1002/2013ja019237.
67. Voss, H.D.; Imhof, W.L.; Walt, M.; Mobilia, J.; Gaines, E.E.; Reagan, J.B.; Inan, U.S.; Helliwell, R.A.; Carpenter, D.L.; Katsufrakis, J.P.; et al. Lightning-induced electron precipitation. *Nature* **1984**, *312*, 740-742, doi:10.1038/312740a0.
68. Rodger, C.J.; Cho, M.G.; Clilverd, M.A.; Rycroft, M.J. Lower ionospheric modification by lightning-EMP: Simulation of the night ionosphere over the United States. *Geophys Res Lett* **2001**, *28*, 199-202, doi:10.1029/2000gl011951.
69. Parrot, M.; Berthelier, J.J.; Lebreton, J.P.; Treumann, R.; Rauch, J.L. DEMETER observations of EM emissions related to thunderstorms. *Space Science Reviews* **2008**, *137*, 511-519, doi:10.1007/s11214-008-9347-y.
70. Parrot, M.; Sauvaud, J.A.; Soula, S.; Pincon, J.L.; van der Velde, O. Ionospheric density perturbations recorded by DEMETER above intense thunderstorms. *J Geophys Res-Space* **2013**, *118*, 5169-5176, doi:10.1002/jgra.50460.
71. Cao, J.; Yang, J.; Yuan, S.; Shen, X.; Liu, Y.; Yan, C.; Li, W.; Chen, T. In-flight observations of electromagnetic interferences emitted by satellite. *Science in China Series E-Technological Sciences* **2009**, *52*, 2112-2118, doi:10.1007/s11431-009-0101-9.
72. Zhima, Z.; Shen, X.; Zhang, X.; Cao, J.; Huang, J.; Ouyang, X.; Jing, L.; Lu, B. Possible Ionospheric Electromagnetic Perturbations Induced by the Ms7.1 Yushu Earthquake. *Earth Moon Planets* **2012**, *108*, 231-241, doi:10.1007/s11038-012-9393-z.
73. Chen, L.; Santolik, O.; Hajos, M.; Zheng, L.; Zhima, Z.; Heelis, R.; Hanzelka, M.; Horne, R.B.; Parrot, M. Source of the low-altitude hiss in the ionosphere. *Geophys Res Lett* **2017**, *44*, 2060-2069, doi:10.1002/2016gl072181.
74. Chen, L.; Pfaff, R.; Heelis, R.; Boardsen, S.; Xia, Z. Ion Cyclotron Resonant Absorption Lines in ELF Hiss Power Spectral Density in the Low-Latitude Ionosphere. *Geophys Res Lett* **2020**, *47*, e2019GL086315, doi:10.1029/2019gl086315.

75. Sauvaud, J.A.; Maggiolo, R.; Jacquey, C.; Parrot, M.; Berthelier, J.J.; Gamble, R.J.; Rodger, C.J. Radiation belt electron precipitation due to VLF transmitters: Satellite observations. *Geophys Res Lett* **2008**, *35*, L09101, doi:10.1029/2008gl033194.
76. Gamble, R.J.; Rodger, C.J.; Clilverd, M.A.; Sauvaud, J.-A.; Thomson, N.R.; Stewart, S.L.; McCormick, R.J.; Parrot, M.; Berthelier, J.-J. Radiation belt electron precipitation by man-made VLF transmissions. *J Geophys Res-Space* **2008**, *113*, A10211, doi:10.1029/2008ja013369.
77. Li, X.; Ma, Y.; Wang, P.; Wang, H.; Lu, H.; Zhang, X.; Huang, J.; Shi, F.; Yu, X.; Xu, Y.; et al. Study of the North West Cape electron belts observed by DEMETER satellite. *Journal of Geophysical Research: Space Physics* **2012**, *117*, A04201, doi:10.1029/2011ja017121.
78. Selesnick, R.S.; Albert, J.M.; Starks, M.J. Influence of a ground-based VLF radio transmitter on the inner electron radiation belt. *Journal of Geophysical Research: Space Physics* **2013**, *118*, 628-635, doi:10.1002/jgra.50095.
79. Sauvaud, J.A.; Walt, M.; Delcourt, D.; Benoist, C.; Penou, E.; Chen, Y.; Russell, C.T. Inner radiation belt particle acceleration and energy structuring by drift resonance with ULF waves during geomagnetic storms. *J Geophys Res-Space* **2013**, *118*, 1723-1736, doi:10.1002/jgra.50125.
80. Sauvaud, J.A.; Parrot, M.; Slominska, E. Comment on "Comparative study on earthquake and ground based transmitter induced radiation belt electron precipitation at middle latitude", by Sideropoulos et al. (2011). *Nat Hazard Earth Sys* **2014**, *14*, 1-9, doi:10.5194/nhess-14-1-2014.
81. Galvan, D.A.; Komjathy, A.; Hickey, M.P.; Stephens, P.; Snively, J.; Song, Y.T.; Butala, M.D.; Mannucci, A.J. Ionospheric signatures of Tohoku-Oki tsunami of March 11, 2011: Model comparisons near the epicenter. *Radio Sci* **2012**, *47*, RS4003, doi:10.1029/2012rs005023.
82. Tsuda, T.; Murayama, Y.; Nakamura, T.; Vincent, R.A.; Manson, A.H.; Meek, C.E.; Wilson, R.L. Variations of the gravity wave characteristics with height, season and latitude revealed by comparative observations. *Journal of Atmospheric and Terrestrial Physics* **1994**, *56*, 555-568, doi:10.1016/0021-9169(94)90097-3.
83. Sun, Y.-Y.; Liu, J.-Y.; Lin, C.-Y.; Tsai, H.-F.; Chang, L.C.; Chen, C.-Y.; Chen, C.-H. Ionospheric F-2 region perturbed by the 25 April 2015 Nepal earthquake. *J Geophys Res-Space* **2016**, *121*, 5778-5784, doi:10.1002/2015ja022280.
84. Chou, M.-Y.; Cherniak, I.; Lin, C.C.H.; Pedatella, N.M. The Persistent Ionospheric Responses Over Japan After the Impact of the 2011 Tohoku Earthquake. *Space Weather* **2020**, *18*, e2019SW002302, doi:10.1029/2019sw002302.
85. Yang, S.-S.; Potirakis, S.M.; Sasmal, S.; Hayakawa, M. Natural Time Analysis of Global Navigation Satellite System Surface Deformation: The Case of the 2016 Kumamoto Earthquakes. *Entropy-Switz* **2020**, *22*, 674, doi:10.3390/e22060674.
86. Chen, C.-H.; Lin, L.-C.; Yeh, T.-K.; Wen, S.; Yu, H.; Yu, C.; Gao, Y.; Han, P.; Sun, Y.-Y.; Liu, J.-Y.; et al. Determination of Epicenters before Earthquakes Utilizing Far Seismic and GNSS Data: Insights from Ground Vibrations. *Remote Sensing* **2020**, *12*, 3252, doi:10.3390/rs12193252.
87. Chen, C.-H.; Lin, J.-Y.; Gao, Y.; Lin, C.-H.; Han, P.; Chen, C.-R.; Lin, L.-C.; Huang, R.; Liu, J.-Y. Magnetic Pulsations Triggered by Microseismic Ground Motion. *J Geophys Res-Sol Ea* **2021**, *126*, doi:10.1029/2020jb021416.
88. Chen, C.-H.; Sun, Y.-Y.; Lin, L.-C.; Han, P.; Yu, H.-Z.; Zhang, X.; Tang, C.-C.; Chen, C.-R.; Yen, H.-Y.; Lin, C.-H.; et al. Large air pressure changes triggered by P-SV ground motion in a cave in northern Taiwan. *Scientific Reports* **2021**, *11*, doi:10.1038/s41598-021-92216-w.
89. Astafyeva, E. Ionospheric Detection of Natural Hazards. *Reviews of Geophysics* **2019**, *57*, 1265-1288, doi:10.1029/2019rg000668.
90. Astafyeva, E.; Shults, K. Ionospheric GNSS Imagery of Seismic Source: Possibilities, Difficulties, and Challenges. *J Geophys Res Space Phys* **2019**, *124*, 534-543, doi:10.1029/2018JA026107.
91. Hutchings, S.J.; Mooney, W.D. The Seismicity of Indonesia and Tectonic Implications. *Geochemistry, Geophysics, Geosystems* **2021**, *22*, doi:10.1029/2021gc009812.

587 92. Pierce, E.T. Atmospheric electricity and earthquake prediction. *Geophys Res Lett* **1976**, *3*, 185-188,
588 doi:10.1029/GL003i003p00185.
589 93. Garavaglia, M.; Dal Moro, G.; Zadro, M. Radon and tilt measurements in a seismic area: Temperature effects. *Physics and*
590 *Chemistry of the Earth Part a-Solid Earth and Geodesy* **2000**, *25*, 233-237, doi:10.1016/s1464-1895(00)00038-7.
591 94. Dey, S.; Singh, R.P. Surface latent heat flux as an earthquake precursor. *Nat Hazard Earth Sys* **2003**, *3*, 749-755,
592 doi:10.5194/nhess-3-749-2003.
593 95. Silva, A.A.; Claro, L.H. Surface air radon progeny at Sao Jose dos Campos, Brazil. *Atmospheric Environment* **2005**, *39*, 4619-
594 4625, doi:10.1016/j.atmosenv.2005.04.025.
595 96. Pulinets, S.A.; Ouzounov, D.; Karelin, A.V.; Boyarchuk, K.A.; Pokhmelnykh, L.A. The physical nature of thermal anomalies
596 observed before strong earthquakes. *Phys Chem Earth* **2006**, *31*, 143-153, doi:10.1016/j.pce.2006.02.042.
597 97. Pulinets, S.; Ouzounov, D. Lithosphere-Atmosphere-Ionosphere Coupling (LAIC) model - An unified concept for
598 earthquake precursors validation. *J Asian Earth Sci* **2011**, *41*, 371-382, doi:10.1016/j.jseaes.2010.03.005.
599 98. Surkov, V.V. Pre-seismic variations of atmospheric radon activity as a possible reason for abnormal atmospheric effects.
600 *Ann Geophys-Italy* **2015**, *58*, doi:10.4401/ag-6808.
601 99. Akhoondzadeh, M.; De Santis, A.; Marchetti, D.; Piscini, A.; Cianchini, G. Multi precursors analysis associated with the
602 powerful Ecuador (M-w=7.8) earthquake of 16 April 2016 using Swarm satellites data in conjunction with other multi-
603 platform satellite and ground data. *Adv Space Res* **2018**, *61*, 248-263, doi:10.1016/j.asr.2017.07.014.
604 100. De Santis, A.; Abbattista, C.; Alfonsi, L.; Amoruso, L.; Campuzano, S.A.; Carbone, M.; Cesaroni, C.; Cianchini, G.; De
605 Franceschi, G.; De Santis, A.; et al. Geosystemics View of Earthquakes. *Entropy-Switz* **2019**, *21*, doi:10.3390/e21040412.
606 101. Zhang, Y.; Meng, Q.; Ouillon, G.; Zhang, L.; Hu, D.; Ma, W.; Sornette, D. Long-term statistical evidence proving the
607 correspondence between tir anomalies and earthquakes is still absent. *European Physical Journal-Special Topics* **2021**, *230*, 133-
608 150, doi:10.1140/epjst/e2020-000248-4.
609 102. Chen, C.-H.; Sun, Y.-Y.; Lin, K.; Zhou, C.; Xu, R.; Qing, H.; Gao, Y.; Chen, T.; Wang, F.; Yu, H.; et al. A New Instrumental
610 Array in Sichuan, China, to Monitor Vibrations and Perturbations of the Lithosphere, Atmosphere, and Ionosphere. *Surv*
611 *Geophys* **2021**, *42*, 1425-1442, doi:10.1007/s10712-021-09665-1.

612